Provided for non-commercial research and education use.
Not for reproduction, distribution or commercial use.

(This is a sample cover image for this issue. The actual cover is not yet available at this time.)

This article appeared in a journal published by Elsevier. The attached copy is furnished to the author for internal non-commercial research and education use, including for instruction at the authors institution and sharing with colleagues.

Other uses, including reproduction and distribution, or selling or licensing copies, or posting to personal, institutional or third party websites are prohibited.

In most cases authors are permitted to post their version of the article (e.g. in Word or Tex form) to their personal website or institutional repository. Authors requiring further information regarding Elsevier's archiving and manuscript policies are encouraged to visit:

http://www.elsevier.com/copyright

Author's personal copy

Journal of Theoretical Biology 300 (2012) 134–142

Contents lists available at SciVerse ScienceDirect

Journal of Theoretical Biology

journal homepage: www.elsevier.com/locate/yjtbi

Front dynamics in a two-species competition model driven by Lévy flights

Emmanuel Hanert *

Université catholique de Louvain, Earth and Life Institute, Environmental Sciences, Croix du Sud 2 bte L7.05.16, B-1348 Louvain-la-Neuve, Belgium

ARTICLE INFO

Article history:
Received 9 May 2011
Received in revised form
24 October 2011
Accepted 12 January 2012
Available online 23 January 2012

Keywords:
Lotka–Volterra model
Lévy flights
Anomalous diffusion
Fractional derivatives
Front dynamics

ABSTRACT

A number of recent studies suggest that many biological species follow a Lévy random walk in their search for food. Such a strategy has been shown to be more efficient than classical Brownian motion when resources are scarce. However, current diffusion–reaction models used to describe many ecological systems do not account for the superdiffusive spread of populations due to Lévy flights. We have developed a model to simulate the spatial spread of two species competing for the same resources and driven by Lévy flights. The model is based on the Lotka–Volterra equations and has been obtained by replacing the second-order diffusion operator by a fractional-order one. Consistent with previous known results, theoretical developments and numerical simulations show that fractional-order diffusion leads to an exponential acceleration of the population fronts and a power-law decay of the fronts' leading tail. Depending on the skewness of the fractional derivative, we derive catch-up conditions for different types of fronts. Our results indicate that second-order diffusion–reaction models are not well-suited to simulate the spatial spread of biological species that follow a Lévy random walk as they are inclined to underestimate the speed at which these species propagate.

© 2012 Elsevier Ltd. All rights reserved.

1. Introduction

In their search for food, many animals do random searches as their detective and cognitive skills are often quite limited with respect to the distribution of their targets (Viswanathan et al., 2008). In such cases, the search for food becomes essentially a stochastic process which has to be as efficient as possible for the forager to survive and thrive. Viswanathan et al. (1999) have shown that Lévy random walks (RWs) maximize the chance of encountering randomly distributed targets when their concentration is low. Although some of the observations of Lévy foraging patterns are still questioned (Edwards et al., 2007; Edwards, 2011; James et al., 2011), different studies suggest that this search strategy has been adopted by many species in response to patchy resource distribution. This is for instance the case for jackals (Atkinson et al., 2002), spider monkeys (Boyer et al., 2006), honey bees (Reynolds et al., 2007a,b), fruit flies (Reynolds and Frye, 2007) and large marine predators (Sims et al., 2008; Humphries et al., 2010). Some observations also seem to suggest that some fishing boats might adopt a Lévy RW search strategy to maximize anchovy catches (Bertrand et al., 2005). The recent book by Viswanathan et al. (2011) gives an extensive review of Lévy RW searches and foraging in biology and ecology.

Observations of Lévy foraging patterns suggest that the movement of living organisms cannot always be represented by a second-order diffusion–reaction model, which rely on the Brownian motion hypothesis (see for instance Okubo and Levin, 2002). In the case of a Brownian RW, the mean square displacement grows linearly, *i.e.* $\langle x^2 \rangle \sim t$. However, for a Lévy RW, the mean square displacement grows superlinearly as $\langle x^2 \rangle \sim t^{2/\alpha}$, where $\alpha < 2$, which results in superdiffusion. Superdiffusion is characterized by a heavy-tailed jump length distribution resulting in diverging spatial moments. With such a distribution, arbitrarily large steps occur with a power-law frequency, in contrast to classical Brownian RW for which large steps are exponentially rare. At the macroscopic level, the population dynamics can then no longer be represented by a second-order diffusion–reaction model. A fractional-order diffusion–reaction model must be used instead (Chaves, 1998; Metzler and Klafter, 2000).

Fractional-order diffusion–reaction models rely on non-local integro-differential operators (Oldham and Spagnier, 1974; Podlubny, 1999), which can be used both for the time and space derivative. On the one hand, time-fractional derivatives of order less than one have been used to represent non-Markovian memory effects leading to subdiffusion. On the other hand, space-fractional derivatives of order less than two have been used to represent long-range dispersion leading to superdiffusion (Metzler and Klafter, 2000, 2004). Space and/or time fractional-order diffusion–reaction models have received an increasing attention in recent years and have been used to model a wide range of problems in surface and subsurface hydrology

* Tel.: +32 10472620; fax: +32 10478898.
E-mail address: emmanuel.hanert@uclouvain.be

0022-5193/$ - see front matter © 2012 Elsevier Ltd. All rights reserved.
doi:10.1016/j.jtbi.2012.01.022

Author's personal copy

(Pachepsky et al., 2003; Deng et al., 2006; Kim and Kavvas, 2006), plasma turbulence (del Castillo Negrete et al., 2004, 2005), finance (Scalas et al., 2000; Cartea and del Castillo Negrete, 2007b), epidemiology (Brockmann, 2009; Hanert et al., 2011) and biology (Raghib et al., 2010; Das and Gupta, 2011). Interestingly, space-fractional diffusion models are related to discrete-time integro-difference models that represent diffusion as a convolution with a dispersal kernel. Classical diffusion corresponds to a Gaussian kernel while the kernel corresponding to space-fractional diffusion is a stable Lévy density function (Baeumer et al., 2007). Several studies have shown that integro-difference models are well suited to simulate biological and ecological phenomena and result in more realistic spreading rates (Kot et al., 1996; Lee et al., 2001; Medlock and Kot, 2003).

While there has been a large interest in Lévy foraging patterns in recent years, very little has been done to adapt the diffusion–reaction models for interacting populations to Lévy flights. All these models are based on the classical Lotka–Volterra model and still assume that individuals in each populations follow a Brownian RW (see Volpert and Petrovskii, 2009 for a review). However, recent studies on fractional-order Fisher–Kolmogorov (del Castillo Negrete et al., 2003) and SIR epidemic models (Hanert et al., 2011) show that the solution dynamics can be deeply modified when replacing the second-order diffusion term by a fractional-order one. In particular, traveling fronts no longer propagate at constant speed but accelerate. The goal of this study is therefore to study the properties of a space-fractional Lotka–Volterra model for two competing species and show how the macroscopic populations dynamics can be modified by Lévy foraging patterns.

The rest of the paper is organized as follows. In the next section, we outline a simple interspecific competition model where the second-order diffusion term has been replaced by a fractional-order one. The impact of fractional-order diffusion on traveling fronts is discussed in Section 3. Depending on the skewness of the fractional derivative, we show that both accelerating and constant-speed fronts can occur and derive catch-up conditions for both types of fronts. A number of numerical examples are provided in Section 4 to confirm the theoretical results and highlight the different front dynamics. The implications of our results are discussed in Section 5.

2. Model description

To illustrate the impact of Lévy foraging patterns on macroscopic population dynamics, we shall consider a two-species Lotka–Volterra competition model with one-dimensional spatial spread. Such a model consists in two coupled diffusion–reaction equations and can be used to represent the spread of an invading species into an area occupied by a competing resident species. The classical form of the model assumes second-order diffusion and is described by the following set of equations:

$$\frac{\partial S_1}{\partial t} = K_1 \frac{\partial^2 S_1}{\partial x^2} + a_1 S_1 (1 - b_{11} S_1 - b_{12} S_2), \tag{1}$$

$$\frac{\partial S_2}{\partial t} = K_2 \frac{\partial^2 S_2}{\partial x^2} + a_2 S_2 (1 - b_{21} S_1 - b_{22} S_2), \tag{2}$$

where, for $i=1,2$, $S_i(x,t)$ are the population densities at position x and time t, a_i are the net birth rates, $1/b_{ii}$ are the carrying capacities, b_{ij} $(j \neq i)$ are the competition coefficients and K_i are the diffusion coefficients (see for instance Murray, 2002a,b).

The second-order diffusion term in Eqs. (1) and (2) results from the assumption that individuals in both populations follow a RW characterized by a finite length scale λ_i and a finite time scale τ_i $(i=1,2)$. Under that assumption, the central limit theorem (CLT) indicates that the probability density function (pdf) of the RW is a Normal distribution characterized by a diffusion coefficient K_i defined as the limit of λ_i^2/τ_i as both scales tend to zero. The Normal distribution representing the density of individuals at time t is in turn the solution of a second-order diffusion equation. Therefore the second-order diffusion equation implicitly assumes that the microscopic individual motion is Brownian, *i.e.* it has finite length and time scales (see for instance Okubo and Levin, 2002).

However, for a Lévy RW there is no typical length scale since arbitrarily large steps can occur with a power-law frequency. The dispersion process is then scale-free and the standard version of the CLT is no more relevant. Instead, the generalization due to Lévy and Gnedenko (Gnedenko and Kolmogorov, 1954; Lévy, 1954) can be used. That version of the CLT does not rely on the assumption that the displacements distribution has a typical length scale but instead assumes it has a power-law tail decaying as $|x|^{-(\alpha+1)}$ with $\alpha \leq 2$. In that case, the pdf of the RW tends towards a stable Lévy distribution with an exponent α (Feller, 1971), which is solution of a diffusion equation of fractional order α (see Metzler and Klafter, 2000 for details). Fig. 1 illustrates the random displacements of a Lévy random walker for different values of the exponent α. It is interesting to note that when $\alpha = 2$, the Lévy motion reduces to a classical Brownian motion.

The generalization of Eqs. (1) and (2) to Lévy motion is achieved by replacing the second-order derivatives by derivatives of fractional-order α_1 and α_2, respectively. For the sake of simplicity, we shall assume that the time dynamics is Markovian (*i.e.* no memory effect), that we have a pure Lévy motion without an upper cutoff (*i.e.* no truncation) and that $1 < \alpha_1, \alpha_2 \leq 2$. The following fractional-order interspecific competition model is then obtained:

$$\frac{\partial S_1}{\partial t} = K_{\alpha_1} \left[\frac{1+\beta_1}{2} {}_{-\infty}D_x^{\alpha_1} S_1 + \frac{1-\beta_1}{2} {}_xD_{+\infty}^{\alpha_1} S_1 \right] + a_1 S_1 (1 - b_{11} S_1 - b_{12} S_2), \tag{3}$$

$$\frac{\partial S_2}{\partial t} = K_{\alpha_2} \left[\frac{1+\beta_2}{2} {}_{-\infty}D_x^{\alpha_2} S_2 + \frac{1-\beta_2}{2} {}_xD_{+\infty}^{\alpha_2} S_2 \right] + a_2 S_2 (1 - b_{21} S_1 - b_{22} S_2), \tag{4}$$

where, for $i=1,2$, the parameters $\beta_i \in [-1, 1]$ are skewness parameters representing a preferential direction of jumps that could result, for instance, from topographical constraints. The left- and right-sided Riemann–Liouville derivatives are defined as

$${}_{-\infty}D_x^{\alpha_i} S_i(x,t) = \mathcal{F}_k^{-1}[(ik)^{\alpha_i} \hat{S}_i(k,t)] = \frac{1}{\Gamma(2-\alpha_i)} \frac{\partial^2}{\partial x^2} \int_{-\infty}^{x} \frac{S_i(y,t)}{(x-y)^{\alpha_i - 1}} \, dy,$$

$${}_xD_{+\infty}^{\alpha_i} S_i(x,t) = \mathcal{F}_k^{-1}[(-ik)^{\alpha_i} \hat{S}_i(k,t)] = \frac{1}{\Gamma(2-\alpha_i)} \frac{\partial^2}{\partial x^2} \int_{x}^{+\infty} \frac{S_i(y,t)}{(y-x)^{\alpha_i - 1}} \, dy,$$

where $\Gamma(\cdot)$ is Euler's gamma function and $\mathcal{F}$ denotes the Fourier transform:

$$\hat{f}(k) = \mathcal{F}_x[f(x)](k) = \int_{-\infty}^{+\infty} f(x) e^{ikx} \, dx.$$

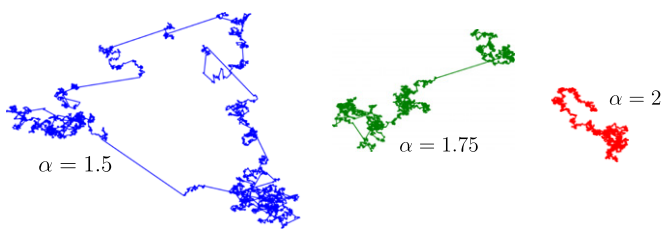

Fig. 1. Illustration of 3 Lévy RW's with different values of the exponent α. Brownian motion is recovered when $\alpha = 2$. The three trajectories have the same number of steps and are represented with the same scaling.

Author's personal copy

The coefficients K_{α_i} are generalized diffusivities that have SI units of $m^{\alpha_i}s^{-1}$. With Eqs. (3) and (4), the spatial spread of both populations is thus governed by the exponents α_i, the diffusivities K_{α_i} and the skewnesses β_i. Finally, the model equations have to be supplemented by a set of initial and boundary conditions to obtain a unique solution. The precise expression of these is not required at this stage.

It is well known that the non-spatial Lotka–Volterra competition model for two species has four possible equilibrium points (S_1^*,S_2^*): $E_1=(0,0)$, $E_2=((1/b_{11}),0)$, $E_3=(0,(1/b_{22}))$ and $E_4=((b_{22}-b_{12})/(b_{11}b_{22}-b_{12}b_{21}),(b_{11}-b_{21})/(b_{11}b_{22}-b_{12}b_{21}))$. The former corresponds to the extinction of both species, the second and the third correspond to the extinction of only one of the two species while the latter is a coexistence state where both species survive. The stability of each of these equilibrium points depends on the sign of the corresponding eigenvalues of the Jacobian matrix

$$J(S_1,S_2)=\begin{pmatrix} a_1(1-2b_{11}S_1-b_{12}S_2) & -a_1b_{12}S_1 \\ -a_2b_{21}S_2 & a_2(1-b_{21}S_1-2b_{22}S_2) \end{pmatrix}. \quad (5)$$

It is then easily seen that E_1 is always unstable while the three other states can be stable for some parameter values (see for instance Shigesada and Kawasaki, 1997 for a discussion). The steady states are obviously not modified by the spatial dynamics of the system. However, we expect the system evolution towards the stable steady state to be modified when using a fractional-order diffusion term rather than a second-order one.

In particular, the existence of Turing patterns and their structure could be modified when replacing the second-order diffusion term by a fractional-order one. This issue has been studied by Gafiychuk and Datsko (2006) and Golovin et al. (2008) who have shown that the Turing mechanism of pattern formation is indeed modified by fractional diffusion as the value of the transition point is changed. For the second-order Lotka–Volterra model of two competing species, it is well known that there are no Turing patterns (see for instance Marchuk et al., 2008). Preliminary results suggest that these patterns are not present neither when $1<\alpha_1,\alpha_2\le 2$.

3. Theoretical analysis

Eqs. (3) and (4) exhibit a variety of traveling wave regimes that depend on the initial conditions and on the model parameters values. To illustrate the impact of fractional-order diffusion on the dynamics of traveling waves of competing species, we shall consider the situation where S_2 represent a species introduced in the wake of S_1 in order to control it, *i.e.* S_1 is an invading species and S_2 is a stronger competitor that has been introduced to eradicate or at least reduce the amplitude of S_1. As mentioned by Shigesada and Kawasaki (1997), the first species eventually disappears if $b_{21}<b_{11}$ and $b_{12}>b_{22}$, while a coexistence steady state is reached if $b_{21}<b_{11}$ and $b_{12}<b_{22}$.

Without loss of generality we will only consider right-propagating fronts. Results for a left-propagating front are entirely symmetric. Initially, both species have a compact support and S_1 is at its carrying capacity, *i.e.* $S_1=1/b_{11}$. The precise expression of the initial condition is not required at this stage. We shall just assume that the support of S_2 is smaller than the support of S_1 and entirely contained within it (see Figs. 3 and 5 for an illustration). The steady states $(0,0)$ and $((1/b_{11}),0)$ will always be unstable for S_2, while $(0,0)$ is always unstable for S_1 (Shigesada and Kawasaki, 1997). With the initial conditions considered here, $(0,0)$ lies just ahead of the S_1 front and $((1/b_{11}),0)$ is just ahead of the S_2 front. It can be seen that the eigenvalues of the Jacobian (5) take their largest value at the steady state $(0,0)$. The maximal growth rate of the reaction term is thus realized at the S_1 front leading, which means that this front is pulled by its leading edge. The model equations can thus be linearized in that region to derive the S_1 front speed. For the S_2 front, there is no guarantee that the leading edge will always correspond to the maximal growth rate of the solution. We therefore make the assumption that the model equations can indeed be linearized at the S_2 leading edge to derive the S_2 front velocity.

Such an assumption has been (implicitly) made in many studies, including the one of Okubo et al. (1989) on the spreading speed of gray squirrels in Britain. However, Hosono (1998) has shown that there are parameter values for which the spreading speed of a second-order Lotka–Volterra competition model is not linearly determined. For that model, Weinberger et al. (2002) and Lewis et al. (2002) have derived a sufficient condition for the linear determinacy of the spreading speed. That result has been further refined by Weinberger et al. (2007). Extending such a linear determinacy condition to fractional-order models is not a trivial task and beyond the scope of this paper. In the remainder of this study, we will therefore assume that the S_2 front speed can be derived by linearizing the model equations at the leading edge. Numerical examples presented in Section 4 suggest that such an assumption is not unrealistic.

The fractional derivative in Eqs. (3) and (4) being a weighted average of the left-sided Riemann–Liouville derivative ${}_{-\infty}D_x^{\alpha}$ and the right-sided one ${}_xD_{+\infty}^{\alpha}$, we shall consider the effect of both derivatives separately. The dispersal kernels corresponding to left- and right-sided derivatives are Lévy distributions with a maximum skewness to the left ($\beta=1$) or to the right ($\beta=-1$), respectively (Baeumer et al., 2007). Such distributions decay algebraically on one side and exponentially on the other (see Fig. 2 for an illustration). In other words, they have a heavy tail on one side and a thin tail on the other side. As mentioned by Kot et al. (1996), the heavy tail leads to accelerating traveling fronts while the thin tail generates constant-speed traveling fronts.

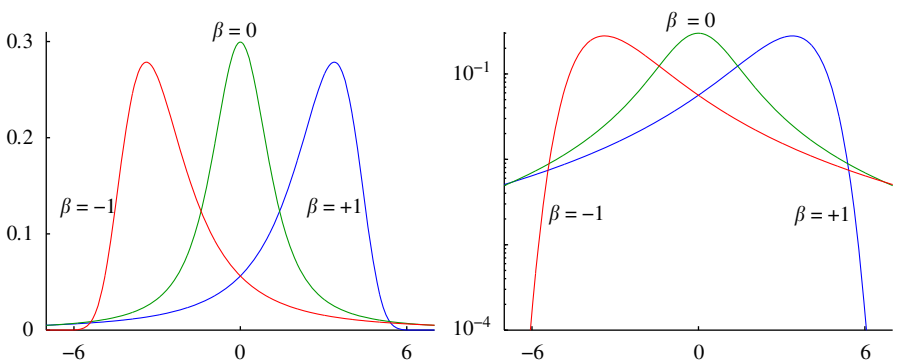

Fig. 2. Example of 3 Lévy distributions with different values of the skewness parameter β and $\alpha=1.2$. The right panel shows the same distributions but with a logarithmic scale for the y-axis. Fully skewed distributions decay algebraically on one side and exponentially on the other.

Author's personal copy

Therefore, in the case of a right-propagating front, the left-sided derivative is expected to accelerate the front while the right-sided derivative shall keep the front speed constant.

3.1. Impact of the left-sided derivative on a right-propagating front

Here we focus only on the impact of the left-sided derivative by taking $\beta_1=\beta_2=1$ in Eqs. (3) and (4). The front speeds are obtained by linearizing the model equations at the leading edge of the corresponding fronts. As mentioned previously, we assume that the S_1 front is ahead of the S_2 front and that S_2 spreads in a region where S_1 is already at its carrying capacity. By linearizing Eq. (3) at the leading edge of the first front, *i.e.* where $S_1\approx 0$ and $S_2\approx 0$, we obtain

$$\frac{\partial S_1}{\partial t}=K_{\alpha_1}({}_{-\infty}D_x^{\alpha_1}S_1)+a_1S_1. \tag{6}$$

Likewise, by linearizing Eq. (4) at the leading edge of the second front, *i.e.* where $S_1\approx 1/b_{11}$ and $S_2\approx 0$, we obtain

$$\frac{\partial S_2}{\partial t}=K_{\alpha_2}({}_{-\infty}D_x^{\alpha_2}S_2)+a_2\left(1-\frac{b_{21}}{b_{11}}\right)S_2. \tag{7}$$

It is readily seen that Eqs. (6) and (7) have the same form as the linearization of the fractional-order Fisher–Kolmogorov equation. Using the same approach as in del Castillo Negrete et al. (2003) and Hanert et al. (2011), the asymptotic solution can be expressed as follows:

$$S_1(x,t)\sim(K_{\alpha_1}t)e^{a_1t}x^{-(\alpha_1+1)}, \tag{8}$$

$$S_2(x,t)\sim(K_{\alpha_2}t)e^{a_2(1-b_{21}/b_{11})t}x^{-(\alpha_2+1)}. \tag{9}$$

As expected, both solutions have a power-law decaying tail of order $-(\alpha_1+1)$ and $-(\alpha_2+1)$, respectively. Interestingly, if one does not assume that S_1 initially has a compact support but instead assumes its support stretches out to $-\infty$, the following asymptotic solution is obtained:

$$S_1(x,t)\sim(K_{\alpha_1}t)e^{a_1t}x^{-\alpha_1}, \tag{10}$$

which has a heavier tail (see Hanert et al., 2011 for details). That would represent the impact of an infinite initial reservoir of individuals from the first species on the traveling front dynamics.

The front speed is obtained by computing the Lagrangian trajectory of a point at the leading edge with a fixed value $\hat{S}_1\approx 0$ and $\hat{S}_2\approx 0$:

$$\hat{x}_1(t)=x(t,\hat{S}_1)\sim\left(\frac{K_{\alpha_1}t}{\hat{S}_1}\right)^{1/(\alpha_1+1)}e^{(a_1/(\alpha_1+1))t},$$

$$\hat{x}_2(t)=x(t,\hat{S}_2)\sim\left(\frac{K_{\alpha_2}t}{\hat{S}_2}\right)^{1/(\alpha_2+1)}e^{(a_2(1-b_{21}/b_{11})/(\alpha_2+1))t}.$$

The front speed, $c_i(t)=\mathrm{d}\hat{x}_i/\mathrm{d}t$, then reads

$$c_1(t)\sim\frac{1}{\alpha_1+1}\left(\frac{K_{\alpha_1}t}{\hat{S}_1}\right)^{1/(\alpha_1+1)}e^{(a_1/(\alpha_1+1))t}\left(a_1+\frac{1}{t}\right), \tag{11}$$

$$c_2(t)\sim\frac{1}{\alpha_2+1}\left(\frac{K_{\alpha_2}t}{\hat{S}_2}\right)^{1/(\alpha_2+1)}e^{(a_2(1-b_{21}/b_{11})/(\alpha_2+1))t}\left(a_2\left(1-\frac{b_{21}}{b_{11}}\right)+\frac{1}{t}\right). \tag{12}$$

Taking into account the effect of Lévy flights in the model therefore leads to exponentially accelerating traveling fronts. This is in agreement with the study of Kot et al. (1996) who found that the solution of integro-difference equations with heavy-tailed kernels that are not exponentially bounded give rise to accelerating fronts. Eqs. (11) and (12) provide a quantitative measure of the exponential rate of acceleration resulting from Lévy dispersion patterns.

From Eqs. (11) and (12), we can derive the following condition under which S_2 catches up with S_1:

$$\frac{a_2(1-b_{21}/b_{11})}{\alpha_2+1}>\frac{a_1}{\alpha_1+1} \tag{13}$$

or

$$\frac{a_2(1-b_{21}/b_{11})}{\alpha_2+1}>\frac{a_1}{\alpha_1}, \tag{14}$$

when S_1 does not have a compact support. Assuming that $b_{21}<b_{11}$, which is required for S_2 to be stronger than S_1, Eqs. (13) and (14) indicate that the key parameters that govern both fronts dynamics are the birth rates a_i ($i=1,2$) and the Lévy exponents α_i ($i=1,2$). Conditions (13) and (14) therefore combine the spatial spread that increases as α_i decreases and the growth rate that triggers an exponential increase as soon as the density value becomes larger than zero. The second species will thus be more likely to control the first one if it can perform larger Lévy flights and if it grows more quickly. Note that once the second species has caught up with the first one or somehow "jumped ahead" of it, it can reach its carrying capacity and the front speeds become

$$c_1(t)\sim\frac{1}{\alpha_1+1}\left(\frac{K_{\alpha_1}t}{\hat{S}_1}\right)^{1/(\alpha_1+1)}e^{(a_1(1-b_{12}/b_{22})/(\alpha_1+1))t}\left(a_1\left(1-\frac{b_{12}}{b_{22}}\right)+\frac{1}{t}\right), \tag{15}$$

$$c_2(t)\sim\frac{1}{\alpha_2+1}\left(\frac{K_{\alpha_2}t}{\hat{S}_2}\right)^{1/(\alpha_2+1)}e^{(a_2/(\alpha_2+1))t}\left(a_2+\frac{1}{t}\right), \tag{16}$$

which means that the S_2 front further accelerates as its exponential acceleration rate becomes $a_2/(\alpha_2+1)$. On the other hand, the exponential acceleration rate of the S_1 front drops to $a_1(1-b_{12}/b_{22})/(\alpha_1+1)$. The S_1 front is thus slowed down and can even be stopped if $b_{12}>b_{22}$.

3.2. Impact of the right-sided derivative on a right-propagating front

A purely right-sided fractional derivative being a global operator on the right-hand side and a local operator on the left-hand side, we expect right-propagating fronts to travel at a constant speed. The front speed is thus derived by following the same approach as with second-order models. By linearizing Eqs. (3) and (4) at the corresponding front leading edge, one obtains linear equations similar to Eqs. (6) and (7) with the exception that the fractional derivative is now right-sided. Dispersion relations $c_i(\kappa)$ can be derived by substituting $S_i\sim\exp(-\kappa(x-c_it))$ in the resulting equations:

$$c_1(\kappa)=\frac{a_1}{\kappa}+\frac{K_{\alpha_1}}{\kappa^{1-\alpha_1}},$$

$$c_2(\kappa)=\frac{a_2(1-b_{21}/b_{11})}{\kappa}+\frac{K_{\alpha_2}}{\kappa^{1-\alpha_2}},$$

where $\kappa>0$ and c_i is the front speed ($i=1,2$). Details of the derivation can be found in del Castillo Negrete et al. (2003) and Hanert et al. (2011).

For a "sufficiently steep" initial condition, fronts propagate at the minimum wave speed $c_{i,min}$ (Ebert and van Saarloos, 2000; van Saarloos, 2003), which is obtained by minimizing c_i with respect to κ:

$$c_{1,min}=\alpha_1K_{\alpha_1}^{1/\alpha_1}\left(\frac{a_1}{\alpha_1-1}\right)^{(\alpha_1-1)/\alpha_1},\quad \kappa_{1,min}=\left(\frac{a_1}{\alpha_1-1}\right)^{1/\alpha_1}, \tag{17}$$

Author's personal copy

$$c_{2,min} = \alpha_2 K_{\alpha_2}^{1/\alpha_2}\left(\frac{a_2(1-b_{21}/b_{11})}{\alpha_2-1}\right)^{(\alpha_2-1)/\alpha_2}, \quad \kappa_{2,min} = \left(\frac{a_2(1-b_{21}/b_{11})}{\alpha_2-1}\right)^{1/\alpha_2}, \tag{18}$$

where $\kappa_{i,min}$ $(i=1,2)$ represents the value of κ that minimizes c_i. van Saarloos (2003) has shown that the front speed algebraically relaxes towards $c_{i,min}$ if the initial condition is steeper than $e^{-\kappa_{i,min}x}$. As mentioned by Ebert and van Saarloos (2000), the algebraic convergence towards the asymptotic front speed is slow, which means that there is no time beyond which convergence can really be neglected. From Eqs. (17) and (18), one can then easily derive the following "catch-up condition":

$$\alpha_2 K_{\alpha_2}^{1/\alpha_2}\left(\frac{a_2(1-b_{21}/b_{11})}{\alpha_2-1}\right)^{(\alpha_2-1)/\alpha_2} > \alpha_1 K_{\alpha_1}^{1/\alpha_1}\left(\frac{a_1}{\alpha_1-1}\right)^{(\alpha_1-1)/\alpha_1},$$

which reduces to the classical result $a_2K_2(1-b_{21}/b_{11}) > a_1K_1$ when $\alpha_1=\alpha_2=2$ (see for instance Volpert and Petrovskii, 2009). Once the second front has caught up with the first one, its speed increases by the factor $(1-b_{21}/b_{11})^{(1-\alpha_2)/\alpha_2}$.

It should be noted that when the skewness coefficients take values strictly between -1 and 1, *i.e.* $-1<\beta_i<1$, both the left- and right-sided derivatives influence the fronts propagation. However, in the case of a right-propagating front, the acceleration resulting from the left-sided derivative will eventually lead to a front speed larger than the constant speed resulting from the right-sided derivative. The macroscopic system dynamics will thus be driven by accelerating fronts. Traveling waves moving at a constant speed should be seen as an exception in systems driven by Lévy flights as they occur only when the fractional-order diffusion term is totally skewed towards the region ahead of the front. For a left-propagating front, acceleration is driven by the right-sided fractional derivative while the left-sided derivative leads to a constant front speed.

4. Numerical results

In this section, we present some numerical simulations that illustrate the theoretical results derived in the previous section. The model equations being solved numerically on a finite domain $[0,L]$, where $L>0$, the fractional-order derivatives ${}_{-\infty}D_x^{\alpha_i}$ and ${}_xD_{+\infty}^{\alpha_i}$ have to be replaced by ${}_0D_x^{\alpha_i}$ and ${}_xD_L^{\alpha_i}$ in Eqs. (3) and (4). The latters are defined as follows:

$${}_0D_x^{\alpha_i} S_i(x,t) = \frac{1}{\Gamma(2-\alpha_i)}\frac{\partial^2}{\partial x^2}\int_0^x \frac{S_i(y,t)}{(x-y)^{\alpha_i-1}}\,\mathrm{d}y,$$

$${}_xD_L^{\alpha_i} S_i(x,t) = \frac{1}{\Gamma(2-\alpha_i)}\frac{\partial^2}{\partial x^2}\int_x^L \frac{S_i(y,t)}{(y-x)^{\alpha_i-1}}\,\mathrm{d}y,$$

where $0\le x\le L$. Solving the model equations on a finite domain might have an impact on the behavior of the solution as fractional-order derivatives are global operators. For compact-support initial conditions, the overall system dynamics is not modified when considering a finite rather than an infinite domain. However, the different front dynamics and the smaller decay rate resulting from an infinite reservoir of individuals cannot be simulated when truncating the computational domain.

One can nevertheless take into account the effect of an infinite reservoir of individuals by slightly modifying the model equations. For instance, to simulate the effect of an infinite reservoir of the first species located at the left-hand side of the domain, one has to replace ${}_0D_x^{\alpha_1} S_1(x,t)$ by ${}_0D_x^{\alpha_1}(S_1(x,t)-S_1(0,t)-\partial S_1/\partial x(0,t))$. This amounts to replace the Riemann–Liouville fractional-order derivative by a Caputo fractional derivative (Podlubny, 1999), which is defined as follows:

$$\begin{aligned}{}_0^CD_x^{\alpha_1} S_1(x,t) &= \frac{1}{\Gamma(2-\alpha)}\int_0^x \frac{\frac{\partial^2 S_1}{\partial y^2}(y,t)}{(x-y)^{\alpha_1-1}}\,\mathrm{d}y \\ &= {}_0D_x^{\alpha_1}\left(S_1(x,t)-S_1(0,t)-\frac{\partial S_1}{\partial x}(0,t)\right).\end{aligned}$$

By using some standard properties of the Caputo derivative, it can be shown that ${}_0^CD_x^{\alpha_1} S_1 = {}_{-\infty}D_x^{\alpha_1} S_1$ if one assumes spatially uniform density values for $x\le 0$, *i.e.* $S_1(x<0,t)=S_1(0,t)$. One can then represent the effect of an infinite reservoir of individuals from the first species at the left-hand side of the domain by selecting an initial condition such that $S_1(0,0)>0$. The same can be done for the right-sided derivative if the infinite reservoir is located at the right-hand side of the domain.

The model equations are discretized in space with a continuous piecewise-linear finite-element scheme on a uniform grid whose resolution is equal to $L/500$. The finite-element scheme is based on a Galerkin formulation that allows one to integrate the fractional-order diffusion term by parts and hence ensure global conservation (see Hanert, 2010 for details). The calculation of the integrals corresponding to the non-linear terms is performed numerically by using a Gaussian quadrature rule. A zero-slope boundary condition is imposed on the left and right boundaries, which allows the fronts to smoothly leave the domain. Time integration is performed with an explicit third-order Adams–Bashforth scheme and the time step is constrained by a CFL-like stability condition that depends on both the reaction and fractional-order diffusion terms. Thanks to the use of an explicit time integration scheme, the non-linear terms in the model equations only have to be evaluated at the previous time step and do not require the use of a non-linear solver.

4.1. Test case 1

This first test case illustrates the two different front dynamics that can arise when the fractional-order diffusion term is totally skewed in one direction. In this example, both fractional derivatives are left-sided, *i.e.* $\beta_1=\beta_2=1$, and both initial conditions are centered in the middle of the domain. They are defined as follows:

$$S_1\left(\frac{2L}{5}\le x\le\frac{3L}{5}\right)=\frac{1}{b_{11}}, \qquad S_2\left(\frac{49L}{100}\le x\le\frac{51L}{100}\right)=\frac{1}{20},$$

$$S_1\left(x<\frac{2L}{5}\right)=\frac{1}{b_{11}}e^{\kappa(2L/5-x)}, \quad S_2\left(x<\frac{49L}{100}\right)=\frac{1}{20}e^{\kappa(49L/100-x)},$$

$$S_1\left(x>\frac{3L}{5}\right)=\frac{1}{b_{11}}e^{-\kappa(x-3L/5)}, \quad S_2\left(x>\frac{51L}{100}\right)=\frac{1}{20}e^{-\kappa(x-51L/100)},$$

where $\kappa=500/L$ and $L=100$. The gridsize Δx is uniform and set to $L/500$. The model parameters take the following values: $\alpha_1=\alpha_2=1.95$, $K_{\alpha_1}=\Delta x^{\alpha_1}/50$, $K_{\alpha_2}=\Delta x^{\alpha_2}/5$, $a_1=0.1$, $a_2=0.2$, $b_{11}=b_{22}=1$, $b_{12}=1.2$, $b_{21}=0.6$, and the simulation duration is set to 500. The expression of the diffusion coefficients K_{α_i} reflects the fact that their physical dimension depends on α_i. With this choice of parameters, the equilibrium state is $(S_1^*,S_2^*)=(0,1)$, which means that the system will evolve towards the extinction of the first species. Finally, it should be noted that even though all the model parameters have well-known physical dimensions, we do not specify any units as our simulations are purely illustrative of the system dynamics and do not intend to reproduce a real system of two competing species.

The centered initial conditions give rise to a left- and a right-propagating front. The fractional derivatives being entirely left-sided, the former travels at a constant speed while the latter is exponentially accelerated. Fig. 3 shows both population densities at different time intervals starting from the initial condition. In this

Author's personal copy

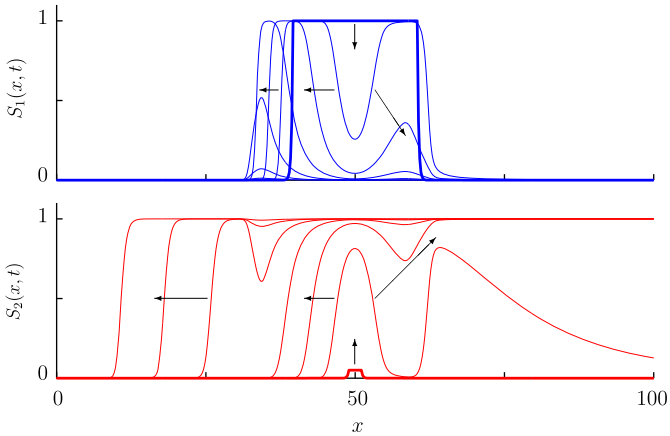

Fig. 3. Left- and right-propagating front profiles arising from an entirely left-sided fractional-order diffusion term. Traveling fronts for both species move to the left at a constant speed and accelerate/decelerate when moving to the right. The S_1 and S_2 population densities are shown at equidistant moments. The arrows indicate the evolution starting from the initial condition represented by a thicker curve.

example, $a_1/(\alpha_1+1)=3.4\times10^{-2}$, $a_2(1-b_{21}/b_{22})/(\alpha_2+1)=\ 2.7\times10^{-2}$ and $a_2/(\alpha_2+1)=6.8\times10^{-2}$. This means that S_2 is slower or at least accelerates less than S_1 in the region where S_1 is still at its carrying capacity, while it is quicker ahead of the S_1 front. However, fractional derivatives being non-local differential operators, they have a far-reaching influence. Therefore, non-zero values of S_2 can appear ahead of the S_1 front, which would subsequently lead to the development of S_2 in a region where S_1 is still small. S_2 being a stronger competitor than S_1, it prevents the development of S_1 ahead of the front. Furthermore, in the region where S_1 is still small, the S_2 front accelerates more than the S_1 front and thus prevents S_1 from "escaping". The dynamics of S_2 can be seen as a consequence of Lévy displacement patterns. Individuals having a non-negligible probability of making large displacements, some of them can "jump ahead" of the region occupied by S_1 and rapidly develop in that region still mostly unoccupied.

The constant speed of the left-propagating front can be obtained from Eqs. (17) and (18): $c_{1,min}=1.8\times10^{-2}$ and $c_{2,min}=5.3\times10^{-2}$. The S_2 front being quicker, it eventually catches up with S_1 and then further increases its speed by $(1-b_{21}/b_{11})^{(1-\alpha_2)/\alpha_2}$ to reach $c_{2,min}=8.3\times10^{-2}$. The speed of the S_2 front can be estimated numerically by tracking the position of a point in the left-propagating front with a density close to zero. For instance, the trajectory $\hat{x}_2(t)$ of the point with the density $S_2=10^{-4}$ is shown in Fig. 4. It shows that the numerical front speed is in good agreement with the theoretical values of $c_{2,min}$ before and after the catch-up.

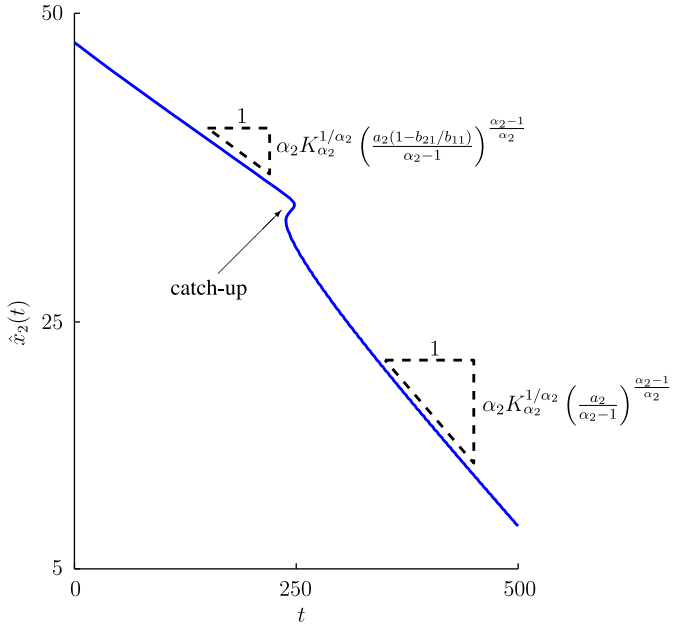

Fig. 4. Time evolution of the left-propagating S_2 front leading edge taken as the Lagrangian trajectory $\hat{x}_2(t)=x(t,S_2=10^{-4})$. The front starts at about $x=48$ and travels at the constant speed $c_{2,min}$ predicted by Eq. (18). After the catch-up with the S_1 front, the S_2 front speed further increases by a factor $(1-b_{21}/b_{11})^{(1-\alpha_2)/\alpha_2}$.

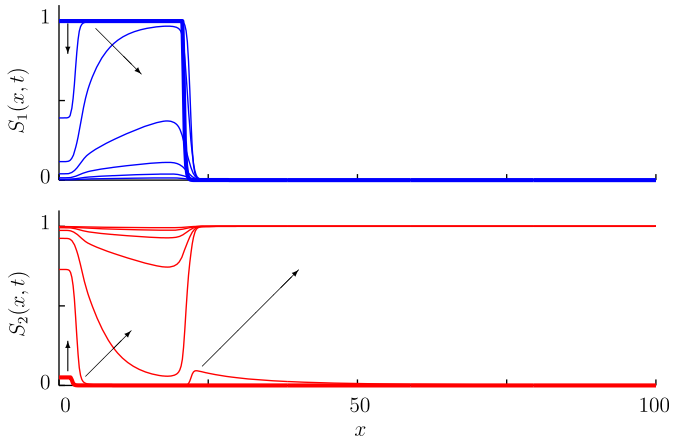

Fig. 5. Right-propagating front profiles leading to the extinction of S_1. The S_2 front spreads more quickly both behind and ahead of the S_1 front, leading to a rapid decline of S_1. Both population densities are shown at equidistant moments. The arrows indicate how the solutions evolve starting from the initial condition represented by a thicker curve.

4.2. Test case 2

In this example, we consider the case where S_2 is both stronger and quicker than S_1. The fractional-order derivatives are now both centered, *i.e.* $\beta_1=\beta_2=0$, which means that diffusion is isotropic. The initial conditions have the following expression:

$$S_1\left(x\le\frac{L}{5}\right)=\frac{1}{b_{11}},\qquad S_2\left(x\le\frac{L}{50}\right)=\frac{1}{20},$$

$$S_1\left(x\ge\frac{L}{5}\right)=\frac{1}{b_{11}}e^{-\kappa(x-L/5)},\quad S_2\left(x\ge\frac{L}{50}\right)=\frac{1}{20}e^{-\kappa(x-L/50)},$$

where $L=100$ and $\kappa=500/L$. The grid resolution is still uniform and equal to $\Delta x=L/500$. The model parameters take the following values: $\alpha_1=1.95$, $\alpha_2=1.8$, $K_{\alpha_i}=\Delta x^{\alpha_i}/50$ $(i=1,2)$, $a_1=0.1$, $a_2=0.3$, $b_{11}=b_{22}=1$, $b_{12}=1.2$, $b_{21}=0.6$, and the simulation duration is set to 300. With this choice of parameters, the equilibrium state is again $(S_1^*,S_2^*)=(0,1)$.

Both populations being initially located in the left corner of the domain, only right-propagating fronts are generated (see Fig. 5). The exponential acceleration of these fronts is governed by the following values: $a_1/(\alpha_1+1)=3.4\times10^{-2}$, $a_2(1-b_{21}/b_{22})/(\alpha_2+1)=\ 4.3\times10^{-2}$ and $a_2/(\alpha_2+1)=1.1\times10^{-1}$. As a result, the S_2 front is quicker than S_1 both in the regions where S_1 is at its carrying capacity and ahead of the S_1 front. S_2 therefore quickly takes over S_1, reaches its carrying capacity and causes the decline of S_1 both ahead and behind the S_1 front (Fig. 5). Fig. 6 shows the same results in logarithmic scale to highlight the power-law decaying tail of both fronts, *i.e.* $S_i\sim x^{-(\alpha_i+1)}$ for $i=1,2$. Furthermore, it shows that the development of S_2 is enhanced as soon as it reaches the region ahead of the S_1 front. The rapid development of S_2 stops the spread of S_1 before leading to its decline.

Author's personal copy

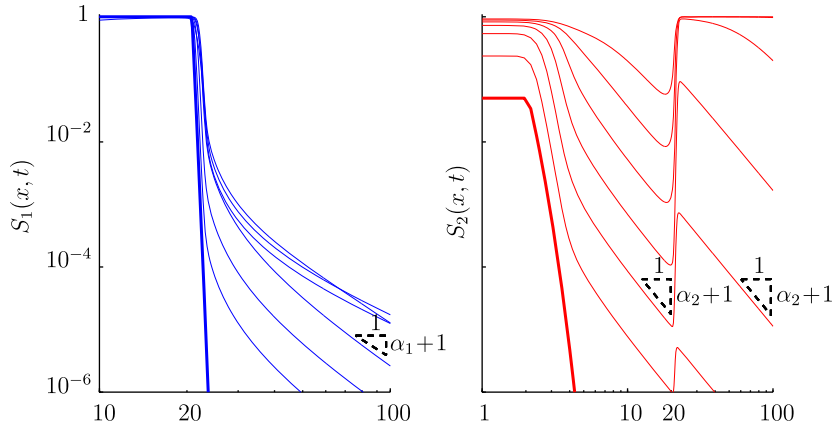

Fig. 6. Same as Fig. 5 but with a logarithmic scale for both axis and a simulation duration equal to 100. The power-law decaying tail of S_1 and S_2 is in agreement with Eqs. (8) and (9), *i.e.* $S_i \sim x^{-(\alpha_i+1)}$ $(i=1,2)$.

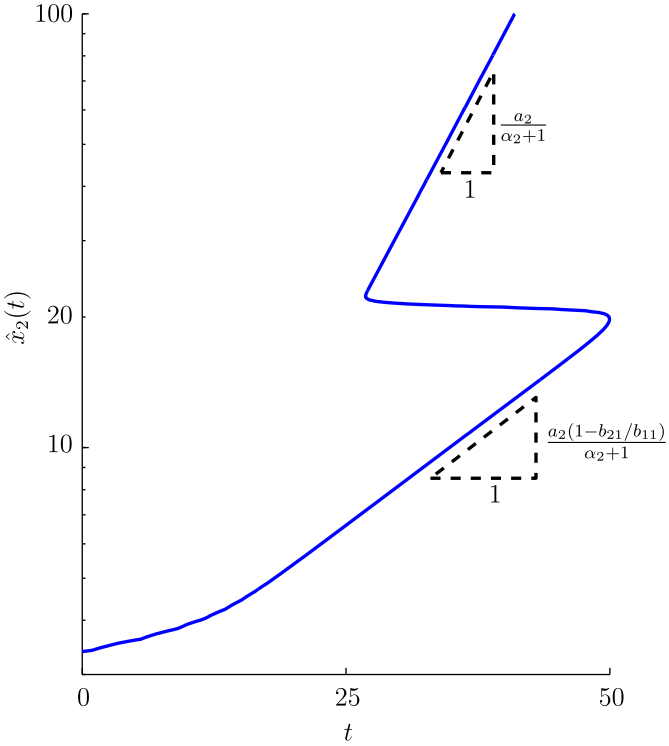

Fig. 7. Time evolution of the right-propagating S_2 front leading edge taken as the Lagrangian trajectory $\hat{x}_2(t)=x(t,S_2=2\times10^{-7})$. The front starts at about $x=3.5$ and accelerates according to Eq. (12), *i.e.* $\hat{x}_2(t)\sim e^{(a_2(1-b_{21}/b_{11})/(\alpha_2+1))t}$. Ahead of the S_1 front, located at about $x=20$, the S_2 front further accelerates in agreement with Eq. (16), *i.e.* $\hat{x}_2(t)\sim e^{a_2/(\alpha_2+1)t}$.

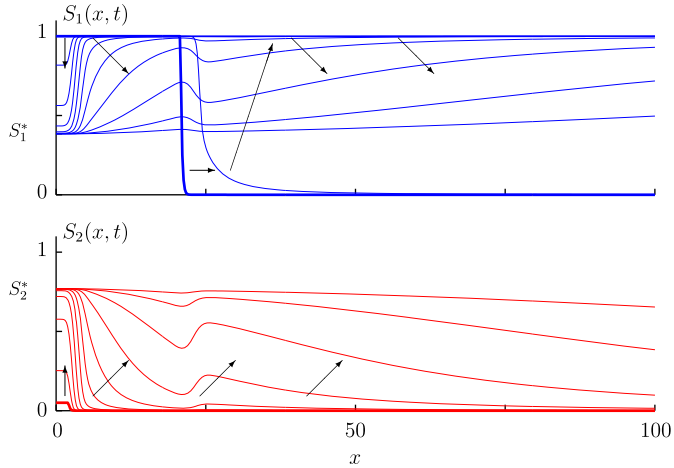

Fig. 8. Right-propagating front profiles leading to a coexistence state between S_1 and S_2. Traveling fronts for both species move to the right but S_1 is much quicker than S_2 and quickly reaches its carrying capacity $(S_1=1)$ before receding towards the coexistence steady state $(S_1=S_1^*)$. Both population densities are shown at equidistant moments. The arrows indicate the evolution starting from the initial condition represented by a thicker curve.

The acceleration of the S_2 front can be estimated numerically by again tracking the position of a point in the front with a density close to zero. The trajectory $\hat{x}_2(t)=x(t,S_2=2\times10^{-7})$ is shown in Fig. 7, where a logarithmic scale has been used for the y-axis. This confirms that behind the S_1 front, located around $x=20$, the S_2 front moves forward as $\hat{x}_2(t)\sim e^{(a_2(1-b_{21}/b_{11})/(\alpha_2+1))t}$. Ahead of the S_1 front, S_2 further accelerates to finally move forward as $\hat{x}_2(t)\sim e^{(a_2/(\alpha_2+1))t}$. Since S_2 can "jump ahead" of S_1, the second leg starts before the first one has reached the S_1 front.

4.3. Test case 3

The final example illustrates the front dynamics that leads to a coexistence steady state when S_2 is slower than S_1, and when there is a infinite reservoir of individuals from the first species at the left-hand side of the domain. To represent the effect of such a reservoir, we replace ${}_0D_x^{\alpha_1}S_1(x,t)$ by ${}_0D_x^{\alpha_1}(S_1(x,t)-S_1(0,t))$. The first-order derivative of S_1 does not have to be taken into account since zero-slope boundary conditions are imposed. The fractional-order diffusion term is centered $(\beta_1=\beta_2=0)$, and the initial conditions and the grid size are the same as for the previous test case. The model parameters take the following values: $\alpha_1=1.8$, $\alpha_2=1.95$, $K_{\alpha_i}=\Delta x^{\alpha_i}/50$ $(i=1,2)$, $a_1=0.3$, $a_2=0.1$, $b_{11}=b_{22}=1$, $b_{12}=0.8$, $b_{21}=0.6$ and the simulation duration is set to 500. With this choice of parameters, the equilibrium state is $(S_1^*,S_2^*)=(0.38,0.77)$, which represents a coexistence state between both species.

The dynamics of the right-propagating fronts is shown in Fig. 8. In this case, the S_1 front is always quicker than the S_2 front as $a_1/\alpha_1=1.7\times10^{-1}$, $a_2(1-b_{21}/b_{22})/(\alpha_2+1)=1.4\times10^{-2}$ and $a_2/(\alpha_2+1)=3.4\times10^{-2}$. As a result, S_1 quickly spreads over the entire domain and reaches its carrying capacity. At that point, the S_1 front has vanished. The S_2 front spreads over the domain with some delay and leads to a decrease of S_1 as both population compete for the same resources. Eventually, the coexistence steady state is reached. The presence of a infinite reservoir of individuals from the first species leads to a higher acceleration of S_1 and also to a smaller rate of decay. The decay rate of S_1 is now $-\alpha_1$ rather than $-(\alpha_1+1)$, while the decay rate of S_2 is still $-(\alpha_2+1)$ (Fig. 9).

Author's personal copy

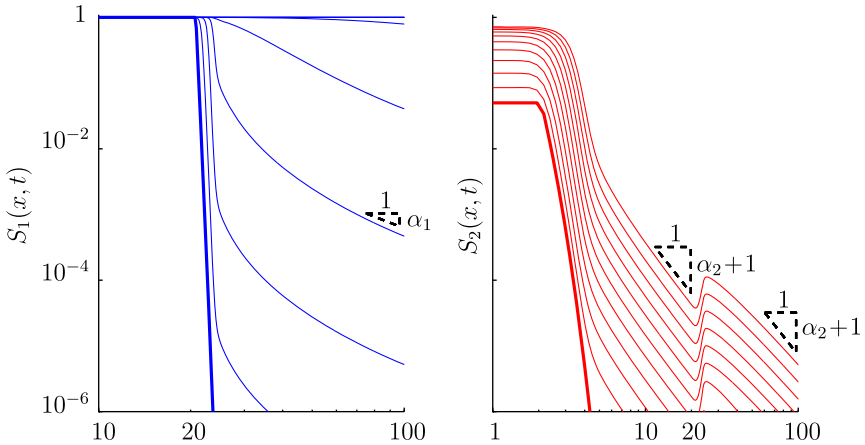

Fig. 9. Same as Fig. 8 but with a logarithmic scale for both axis and a simulation duration equal to 150. The presence of an infinite reservoir of individuals from S_1 at the left-hand side of the domain leads to smaller decay rate in agreement with Eq. (10), *i.e.* $S_1 \sim x^{-\alpha_1}$. The power-law decaying tail of S_2 is not modified, *i.e.* $S_2 \sim x^{-(\alpha_2+1)}$.

The Lagrangian trajectory of the S_2 front leading edge is similar to the one observed in the previous test case (Fig. 7) with the exception that the exponential rate of acceleration is always equal to $a_2(1-b_{21}/b_{11})/(\alpha_2+1)$. This is because S_1 is quicker than S_2 and reaches its carrying capacity in all the region ahead of S_2 without being caught up by S_2. As a result, the S_2 front is never able to reach an acceleration rate equal to $a_2/(\alpha_2+1)$.

5. Conclusions

In this paper, we have proposed a fractional-order interspecific competition model based on the standard Lotka–Volterra model for two species competing for the same resources. Our model takes into account the diffusion process resulting from Lévy foraging patterns, which are optimal as resources are scarce. The importance of Lévy flights is represented in the model by a coefficient $\alpha \leq 2$. When $\alpha = 2$, Brownian motion and thus second-order diffusion are recovered. The superdiffusive effect of Lévy flights and fractional-order diffusion occurs as soon as $\alpha < 2$. The macroscopic system dynamics is strongly influenced by Lévy flights as they give rise to accelerating rather than constant-speed traveling fronts, which are predicted by second-order models. The spatial behavior of the solutions is also modified as they exhibit an algebraically decaying tail typical of long-range interactions. This suggests that second-order diffusion–reaction models are not well suited to represent the spread of populations that follow a Lévy RW. Second-order models are inclined to underestimate the speed at which an invading species propagate.

However, as mentioned by Kot et al. (1996) and Viswanathan et al. (2008), a pure Lévy RW cannot take place in a finite space as there will always be an upper bound on the distance that one individual can travel and on the speed at which the population can spread. Such an upper bound could be introduced in our model by considering truncated Lévy distributions (Mantegna and Stanley, 1994), which amount to introduce a cut-off length beyond which the probability of large displacements decays exponentially. Such distributions thus eliminate arbitrarily large steps produced by Lévy distributions and have finite moments. At the macroscopic level, truncated Lévy distributions translate into truncated fractional-order diffusion models (Cartea and del Castillo Negrete, 2007a). del Castillo Negrete (2009) has studied the front dynamics generated by the truncated fractional-order Fisher–Kolmogorov equation and has shown that exponential acceleration and algebraically decaying tails then only occur in an intermediate asymptotic regime beyond which the front speed converges towards a constant value.

The model could also be improved by taking into account a non-Markovian time dynamics. At the microscopic level, this amounts to consider an algebraically decaying waiting times distribution rather than an exponentially decaying one. At the macroscopic level, it translates into a time-fractional diffusion equation that leads to subdiffusion and memory effects. The numerical solution of such an equation is quite challenging as the entire solution history is needed at each time step. Numerical methods have recently been proposed to discretize the space-time fractional diffusion equation and could be applied in a non-Gaussian and non-Markovian population model (Podlubny et al., 2009; Hanert, 2011).

References

Atkinson, R.P.D., Rhodes, C.J., Macdonald, D.W., Anderson, R.M., 2002. Scale-free dynamics in the movement patterns of jackals. Oikos 98, 134–140.

Baeumer, B., Kovács, M., Meerschaert, M.M., 2007. Fractional reproduction-dispersal equations and heavy tail dispersal kernels. Bull. Math. Biol. 69, 2281–2297.

Bertrand, S., Burgos, J.M., Gerlotto, F., Atiquipa, J., 2005. Lévy trajectories of Peruvian purse-seiners as an indicator of the spatial distribution of anchovy (*Engraulis ringens*). ICES J. Mar. Sci. 62, 477–482.

Boyer, D., Ramos-Fernández, G., Miramontes, O., Mateos, J.L., Cocho, G., Larralde, H., Ramos, H., Rojas, F., 2006. Scale-free foraging by primates emerges from their interaction with a complex environment. Proc. Biol. Sci./R. Soc. 273, 1743–1750.

Brockmann, D., 2009. Human mobility and spatial disease dynamics. In: Schuster, H.G. (Ed.), Reviews of Nonlinear Dynamics and Complexity. Wiley-VCH, pp. 1–24.

Cartea, A., del Castillo Negrete, D., 2007a. Fluid limit of the continuous-time random walk with general Lévy jump distribution functions. Phys. Rev. E—Stat. Nonlinear Soft Matter Phys. 76, 041105.

Cartea, A., del Castillo Negrete, D., 2007b. Fractional diffusion models of option prices in markets with jumps. Phys. A: Stat. Mech. Appl. 374, 749–763.

Chaves, A.S., 1998. A fractional diffusion equation to describe Lévy flights. Phys. Lett. A 239, 13–16.

Das, S., Gupta, P.K., 2011. A mathematical model on fractional Lotka–Volterra equations. J. Theor. Biol. 277, 1–6.

del Castillo Negrete, D., 2009. Truncation effects in superdiffusive front propagation with Lévy flights. Phys. Rev. E 79, 1–10.

del Castillo Negrete, D., Carreras, B.A., Lynch, V.E., 2003. Front dynamics in reaction–diffusion systems with Lévy flights: a fractional diffusion approach. Phys. Rev. Lett. 91.

del Castillo Negrete, D., Carreras, B.A., Lynch, V.E., 2004. Fractional diffusion in plasma turbulence. Phys. Plasmas 11, 3854–3864.

del Castillo Negrete, D., Carreras, B.A., Lynch, V.E., 2005. Nondiffusive transport in plasma turbulence: a fractional diffusion approach. Phys. Rev. Lett. 94.

Deng, Z.Q., de Lima, J.L.M.P., de Lima, M.I.P., Singh, V.P., 2006. A fractional dispersion model for overland solute transport. Water Resour. Res. 42, W03416.

Author's personal copy

Ebert, U., van Saarloos, W., 2000. Front propagation into unstable states: universal algebraic convergence towards uniformly translating pulled fronts. Physica D 146, 1–99.
Edwards, A.M., Phillips, R.A., Watkins, N.W., Freeman, M.P., Murphy, E.J., Afanasyev, V., Buldyrev, S.V., Da-Luz, M.G.E., Raposo, E.P., Stanley, H.E., Viswanathan, G.M., 2007. Revisiting Lévy flight search patterns of wandering albatrosses, bumblebees and deer. Nature 449, 1044–1048.
Edwards, A.M., 2011. Overturning conclusions of Lévy flight movement patterns by fishing boats and foraging animals. Ecology 92, 1247–1257.
Feller, W., 1971. An Introduction to Probability Theory and Its Applications, vol. II. Wiley.
Gafiychuk, V., Datsko, B., 2006. Pattern formation in a fractional reaction–diffusion system. Phys. A: Stat. Mech. Appl. 365, 300–306.
Gnedenko, B., Kolmogorov, A., 1954. Limit Distributions for Sums of Independent Random Variables. Addison-Wesley.
Golovin, A.A., Matkowskyt, B.J., Volpert, V.A., 2008. Turing pattern formation in the Brusselator model with superdiffusion. SIAM J. Appl. Math. 69, 251–272.
Hanert, E., 2010. A comparison of three Eulerian numerical methods for fractional-order transport models. Environ. Fluid Mech. 10, 7–20. doi:10.1007/s10652-009-9145-4.
Hanert, E., 2011. On the numerical solution of space-time fractional diffusion models. Comput. Fluids 46, 33–39. doi:10.1016/j.compfluid.2010.08.010.
Hanert, E., Schumacher, E., Deleersnijder, E., 2011. Front dynamics in fractional-order epidemic models. J. Theor. Biol. 279, 9–16. doi:10.1016/j.jtbi.2011.03.012.
Hosono, Y., 1998. The minimal speed of traveling fronts for a diffusive Lotka–Volterra competition model. Bull. Math. Biol. 60, 435–448.
Humphries, N.E., Queiroz, N., Dyer, J.R.M., Pade, N.G., Musyl, M.K., Schaefer, K.M., Fuller, D.W., Brunnschweiler, J.M., Doyle, T.K., Houghton, J.D.R., Hays, G.C., Jones, C.S., Noble, L.R., Wearmouth, V.J., Southall, E.J., Sims, D.W., 2010. Environmental context explains Lévy and Brownian movement patterns of marine predators. Nature 465, 1066–1069.
James, A., Planck, M.J., Edwards, A.M., 2011. Assessing Lévy walks as models of animal foraging. J. R. Soc. Interface 8, 1233–1247.
Kim, S., Kavvas, M.L., 2006. Generalized Fick's law and fractional ADE for pollution transport in a river: detailed derivation. J. Hydrol. Eng. 11, 80–83.
Kot, M., Lewis, M.A., van den Driessche, P., 1996. Dispersal data and the spread of invading organisms. Ecology 77, 2027–2042.
Lee, C.T., Hoopes, M.F., Diehl, J., Gilliland, W., Huxel, G., Leaver, E.V., McCann, K., Umbanhowar, J., Mogilner, A., 2001. Non-local concepts and models in biology. J. Theor. Biol. 210, 201–219.
Lévy, P., 1954. Théorie de l'Addition des Variables Aléatoires. Gauthier-Villars.
Lewis, M.A., Li, B., Weinberger, H.F., 2002. Spreading speed and linear determinacy for two-species competition models. J. Math. Biol. 45, 219–233.
Mantegna, R.N., Stanley, H.E., 1994. Stochastic process with ultraslow convergence to a Gaussian: the truncated Lévy flight. Phys. Rev. Lett. 73, 2946–2949.
Marchuk, H., Petrovskii, S.V., Venturino, E., 2008. Spatiotemporal Patterns in Ecology And Epidemiology: Theory, Models, and Simulation, Mathematical and Computational Biology Series. Chapman & Hall/CRC.
Medlock, J., Kot, M., 2003. Spreading disease: integro-differential equations old and new. Math. Biosci. 184, 201–222.
Metzler, R., Klafter, J., 2000. The random walk's guide to anomalous diffusion: a fractional dynamics approach. Phys. Rep. 339, 1–77.
Metzler, R., Klafter, J., 2004. The restaurant at the end of the random walk: recent development in the description of anomalous transport by fractional dynamics. J. Phys. A 37, 161–208.
Murray, J., 2002a. Mathematical Biology. I. Introduction. Springer-Verlag, New York.
Murray, J., 2002b. Mathematical Biology. II. Spatial Models and Biomedical Applications. Springer-Verlag, New York.
Okubo, A., Levin, S.A., 2002. Diffusion and Ecological Problems: Modern Perspectives. Interdisciplinary Applied Mathematics. Springer.
Okubo, A., Maini, P.K., Williamson, M.H., Murray, J.D., 1989. On the spatial spread of the gray squirrel in Britain. Proc. R. Soc. London B238, 113–125.
Oldham, K., Spagnier, J., 1974. The Fractional Calculus: Theory and Applications of Differentiation and Integration to Arbitrary Order. Academic Press.
Pachepsky, Y., Timlin, D., Rawls, W., 2003. Generalized Richards' equation to simulate water transport in unsaturated soils. J. Hydrol. 272, 3–13.
Podlubny, I., 1999. Fractional differential equations. Mathematics in Science and Engineering, vol. 198. Academic Press.
Podlubny, I., Chechkin, A., Skovranek, T., Chen, Y., Jara, B.M.V., 2009. Matrix approach to discrete fractional calculus. II. Partial fractional differential equations. J. Comput. Phys. 228, 3137–3153.
Raghib, M., Levin, S., Kevrekidis, I., 2010. Multiscale analysis of collective motion and decision-making in swarms: an advection–diffusion equation with memory approach. J. Theor. Biol. 264, 893–913.
Reynolds, A.M., Frye, M.A., 2007. Free-flight odor tracking in drosophila is consistent with an optimal intermittent scale-free search. PLoS One 2, e354.
Reynolds, A.M., Smith, A.D., Menzel, R., Greggers, U., Reynolds, D.R., Riley, J.R., 2007a. Displaced honey bees perform optimal scale-free search flights. Ecology 88, 1955–1961.
Reynolds, A.M., Smith, A.D., Reynolds, D.R., Carreck, N.L., Osborne, J.L., 2007b. Honeybees perform optimal scale-free searching flights when attempting to locate a food source. J. Exp. Biol. 210, 3763–3770.
Scalas, E., Gorenflo, R., Mainardi, F., 2000. Fractional calculus and continuous-time finance. Phys. A: Stat. Mech. Appl. 284, 376–384.
Shigesada, N., Kawasaki, K., 1997. Biological Invasions: Theory and Practice, Oxford Series in Ecology and Evolution. OUP, Oxford.
Sims, D.W., Southall, E.J., Humphries, N.E., Hays, G.C., Bradshaw, C.J.A., Pitchford, J.W., James, A., Ahmed, M.Z., Brierley, A.S., Hindell, M.A., Morritt, D., Musyl, M.K., Righton, D., Shepard, E.L.C., Wearmouth, V.J., Wilson, R.P., Witt, M.J., Metcalfe, J.D., 2008. Scaling laws of marine predator search behaviour. Nature 451, 1098–1102.
van Saarloos, W., 2003. Front propagation into unstable states. Phys. Rep. 386, 29–222.
Viswanathan, G., Raposo, E., da Luz, M., 2008. Lévy flights and superdiffusion in the context of biological encounters and random searches. Phys. Life Rev. 5, 133–150.
Viswanathan, G.M., Buldyrev, S.V., Havlin, S., Da Luz, M.G.E., Raposo, E.P., Stanley, H.E., 1999. Optimizing the success of random searches. Nature 401, 911–914.
Viswanathan, G.M., da Luz, M.G.E., Raposo, E.P., Stanley, H.E., 2011. The Physics of Foraging. Cambridge University Press.
Volpert, V., Petrovskii, S., 2009. Reaction–diffusion waves in biology. Phys. Life Rev. 6, 267–310.
Weinberger, H.F., Lewis, M.A., Li, B., 2002. Analysis of linear determinacy for spread in cooperative models. J. Math. Biol. 45, 183–218.
Weinberger, H.F., Lewis, M.A., Li, B., 2007. Anomalous spreading speeds of cooperative recursion systems. J. Math. Biol. 55, 207–222.